The immunodominant protein P116 is a passive transporter of cholesterol and other essential lipids

Lasse Sprankel[1,*], David Vizarraga[2,*], Jesús Martín[2], Sina Manger[1], Jakob Meier-Credo[3], Marina Marcos[4], Josep Julve[5], Noemi Rotllan[5], Margot P. Scheffer[1], Joan Carles Escolà-Gil[5], Julian D. Langer[3], Jaume Piñol[4], Ignacio Fita[2,#] and Achilleas S. Frangakis[1,#]

[1]Buchmann Institute for Molecular Life Sciences and Institute of Biophysics, Goethe University Frankfurt, Max-von-Laue Str. 15, 60438 Frankfurt, Germany
[2]Instituto de Biología Molecular de Barcelona (IBMB-CSIC), Parc Científic de Barcelona, Baldiri Reixac 10, 08028 Barcelona, Spain3
[3]Max Planck Institute for Biophysics, Max-von-Laue Str. 15, 60438 Frankfurt, Germany
[4]Institut de Biotecnologia i Biomedicina and Departament de Bioquímica i Biologia Molecular, Universitat Autònoma de Barcelona, 08193 Cerdanyola del Vallès, Spain
[5]Institut de Recerca de l'Hospital de la Santa Creu i Sant Pau and CIBER de Diabetes y Enfermedades Metabólicas Asociadas (CIBERDEM), C/ Sant Quintí 77, 08041 Barcelona, Spain

---

* *These authors contributed equally to this work. Name order was decided randomly. Both authors are entitled to use their names first when citing this work.*

Abstract

Many human pathogens need to extract lipids from their environment for survival and proliferation. How the lipid uptake is accomplished on a molecular level is largely unknown, and no proteins directly involved in this process have been characterized to date. Here, we report a comprehensive structural and functional analysis of the previously uncharacterized protein P116 (MPN_213) from *Mycoplasma pneumoniae*, a human pathogen responsible for approximately 30% of community-acquired human pneumonia. Fluorescence microscopy, using antibodies raised against the ectodomain of P116, shows a ubiquitous distribution of P116 on the cell surface, indicating a direct role in host cell interactions. Single-particle cryo-electron microscopy at 3.3 Å resolution reveals two homodimers connected by a dimerization interface, and a core domain presenting a previously unseen fold. This fold creates a large cavity of ~18,000 $Å^3$ with a fully hydrophobic internal surface that is accessible to solvent. The hydrophobic residues lining the cavity are conserved in P116 orthologues of other *Mycoplasma* species. We also observed elongated densities with a length of 10-19 Å long and a width of 4 Å within the cavity, which are not accounted for by the structure and which we identified as the essential lipids phosphatidylcholine, sphingomyelin and cholesterol using mass spectrometry. When the cavity is emptied by stringent treatment with detergents, the protein undergoes an extensive conformational change to adopt a closed conformation that no longer allows for the accommodation of lipids. We conducted radioactivity transfer experiment demonstrating a net transfer of cholesterol from high-density lipoproteins (HDLs) to P116, and observed an uptake of cholesterol into previously-emptied P116 from serum. We also found a direct attachment of P116 to HDLs using cryo-electron microscopy. These results reveal the mechanism by which P116 captures essential lipids from the host environment and possibly then delivers them by a wringing movement into the membrane by passive transport.

Introduction

Mycoplasma pneumoniae is a facultative intracellular human pathogen causing community-acquired pneumonia that can manifest severe systemic effects[1]. Unlike other respiratory pathogens, *M. pneumoniae* has no approved vaccine[2]. *Mycoplasmas* lack a cell wall and have the smallest known genomes[3]. *M. pneumoniae*, with a 816 kb genome, is a model organism for a minimal cell[4]. Many of the metabolic pathways required to synthesize essential products are absent, which makes uptake by specialized mechanisms necessary. *M. pneumoniae* cannot synthesize several of the lipids that are important components of the cell membrane, such as sphingomyelin, phosphatidylcholine and cholesterol[5]. Instead, it must take up lipids from the host environment. The membrane composition of *M. pneumoniae* changes depending on the medium composition in vitro[6–8], and *M. pneumoniae* can use a wide range of lipids and survive. Cholesterol, which is present in only a few prokaryotes including the clinically relevant Helicobacter pylori and Borrelia *burgdorferi*, is essential for *M. pneumoniae* cells and is the most abundant lipid in the membranes, accounting for 35–50% of the total lipid fraction[8]. However, it is unclear how *Mycoplasma* and other prokaryotic species that depend on lipid uptake from the environment for their survival achieve the uptake of lipid species and incorporate them into their membrane[9].

In this work, we report the structural and functional characterization of P116, an essential protein for the viability of *M. pneumoniae* cells. P116 was previously uncharacterized, although it has been reported to potentially contribute to adhesion to host cells[10]. Despite the essential role of P116 and its strong immunogenicity, the *M. pneumoniae* genome contains only a single copy of *p116* (*mpn213*). We first determined the structure of the P116 ectodomain by single-particle cryo-electron microscopy (cryoEM). The structure has a novel fold (with no matches in the Protein Data Bank) featuring a uniquely large hydrophobic cavity that is fully accessible to solvent. Mass spectrometry and other analytical techniques identify the ligands as several different lipids, some of which are essential. Based on these findings, we describe the mechanism by which *Mycoplasmas* can extract lipids from the environment and possibly also deposit them in their own membrane, thus explaining the essential role of P116 for the survival of *M. pneumoniae* cells.

Results

P116 is abundant on the cell surface

A construct predicted to span the whole ectodomain of P116 from *M. pneumoniae* (residues 30–957) was overexpressed in *Escherichia coli* and purified by His-tag affinity and gel filtration chromatography (Materials and Methods and **Supplementary Figure 1**). Immunolabeling with both polyclonal and monoclonal antibodies against this construct showed an intense and uniform distribution of labeling across the whole surface of *M. pneumoniae* cells (**Figure 1A**), with adhesion and motility unaffected by the antibodies. This distribution contrasts with that of P1, an adhesion protein that concentrates at the tip of the cell and has strong effects on adhesion and motility[11,12].

P116 has a novel fold with a lipid-accessible cavity

The structure of P116(30–957) was determined by single-particle cryoEM at 3.3 Å resolution (according to the gold standard criterion of FSC 0.143; **Supplementary Table I**, **Supplementary Figure 2**. It is an elongated homodimer of ~240 Å along its longest axis, which adopts an arched shape with an arc-radius of 200 Å (**Figure 1B**, **Movies 1, 2**). Each monomer consists of two distinct subunits: an N-terminal domain (residues 60–245), situated distal to the dimer axis, and a core domain (residues 246–867). Proximal to the dimer axis is the dimerization interface (**Figure 1B**, **Supplementary Figure 3**), which is very well resolved. In addition, the N-terminal domain has significant hinge mobility with respect to the core domain, which reduced the local resolution of the cryoEM map (**Supplementary Figure 2**), making model building difficult for the most distal parts of the construct (see Materials and Methods and **Supplementary Figure 4**). The homodimer displays significant flexibility with many vibrational modes, as classification illustrates (**Supplementary Figure 5**). Finally, some residues at the N- and C-termini of the construct (30–59 and 868–957, respectively) were not visible in the cryoEM maps. The flexibility of the homodimer involves a change in the curvature of approximately 100 Å, wringing along the axis perpendicular to the dimer axis by ~80 degrees, and bending up to 20 degrees (**Supplementary Figure 5, Movie 3**).

The core domain resembles a half-opened left hand, with four contiguous antiparallel α-helices corresponding to the four fingers (**Figure 2A**). The helices corresponding to the wrist form the dimer interface, and a conserved tryptophan residue (Trp681) interacts tightly with the neighboring monomer. In the variant Trp681Ala, the rate of dimers to monomers is 1:4, compared to only dimers without the mutation (**Supplementary Figure 3b**). The palm of the hand includes a long and well defined central α-helix, the bridge helix (residues 268–304), and a rigid β-sheet of five antiparallel strands that extends to the N-terminal domain (**Figure 2B**). The hand appears in a half-opened state with a large elongated cleft across the whole core domain. The inner part of the hand (i.e. the fingers and palm) forms a large cavity that measures 62 Å proximal to distal and 38 Å anterior to posterior with a volume of ~18,000 $Å^3$.

The cavity is completely hydrophobic although fully accessible to the solvent (**Figure 2B** , **Movie 4)**. In addition, the core has two access points, one at the dorsal side and one at the distal side (**Figure 3**). Using the DALI server, we found only very weak structural relationships between P116 and all other experimentally determined protein structures available in the Protein Data Bank, which shows that P116 has a new, unique fold.

The N-terminal domain is compact and organized around a cluster of aromatic residues, at the center of which is the only tryptophan residue of the domain (Trp121). The N-terminal and core domains of P116 superimpose for 126 equivalent residues (68% of the N-terminal domain), suggesting that P116 might have been generated by duplication of an ancestor domain**.** The common secondary structural elements in the N-terminal and core domains consist of a β-sheet and the two helices preceding the sheet (**Figure 2B**). The core domain is much larger than the N-terminal domain mainly due to two insertions containing twelve and four helices, respectively.

For the inner part of the P116 core domain, the cryoEM maps show prominent elongated densities (with a length of 10–19 Å and a width of 4 Å) that fill most of the hydrophobic areas (**Figure 3A**, **Movies 5, 6**). These elongated densities, which are unaccounted for, cannot be explained by the protein residues missing in the model. Instead, the mass excess of ~13 kDa, consistently measured by MALS and mass spectrometry for P116 in different preparations, could be explained by the presence of ligand molecules bound to P116 (**Figure 4a**). Initial mass spectrometry analysis of the same samples from which the structure of P116 was determined (see Materials and Methods) showed the presence of several lipid species, including phosphatidylcholine and sphingomyelin, which are essential for *M. pneumoniae*[3], and of wax esters (**Figure 4b and Supplementary Figure 6**).

Among the P116 orthologues found in a BlastP search[13] of eight *Mycoplasma* species, the amino acids lining the hydrophobic cavity are largely conserved (either identical or with similar characteristics), in particular those in the proximity of the unaccounted, elongated densities (**Supplementary Figure 7**). Modeling P116 and its orthologues with AlphaFold[14] results in all the models having a similar tertiary structure, in which a large core domain is flanked by a smaller N-terminal domain, but the relative position of the domains does not closely match the experimental structure.

The conformation of empty P116 cannot accommodate lipid binding

To obtain ‘empty’ P116 that was free of any bound ligands, we treated the P116 samples with the detergent Triton-X 100 (see below and Materials and Methods). Mass

spectrometry confirmed a massive reduction of lipids in the sample (**Figure 4b)**. The structure of the empty P116 sample was solved by cryoEM at 4 Å resolution (**Supplementary Figure 8**). Its overall topology is almost identical to that of the original P116 sample, with the difference that the cavity is closed as a result of fingers 1, 2 and 3 being closer to the palm by 8, 13 and 12 Å, respectively, and finger 4 moving 11 Å sideways to retain the distal core access to the palm (**Figure 3b**, **Movies 7**, **8**, and **Supplementary Figure 9**). These changes reduce the volume within the core domain from ~18,000 $Å^3$ to ~6,300 $Å^3$. The unoccupied volume between the fingers and palm reduces to two pockets that are large enough for small lipids to pass through but appear unoccupied in the cryoEM density. A comparison of the filled and empty P116 structures shows that the original densities that were unaccounted for create massive steric clashes in the closed configuration of the fingers, demonstrating that the cavity can no longer accommodate lipids (**Movie 9**). In the empty P116, the dimerization interface is shifted towards the dorsal side of the molecule by 10 Å, resulting in a contraction that changes the arc radius of the dimer from 500 to 600 Å and shifts the N-terminal domain towards the dimerization interface.

Refilled P116 is structurally identical to the purified sample

We next refilled the empty P116 samples by incubating them either with fetal bovine serum (FBS) or with high-density lipoproteins (HDL) and then re-purified them by affinity chromatography. Media containing FBS is a common growing broth for *M. pneumoniae* cultures, although lipoproteins, in particular HDL, are efficient substitutes for serum in *Mycoplasma* culture media, likely because lipoproteins can provide the key lipids, in particular cholesterol, which is essential for *Mycoplasma* cells[15]. We solved the structure of the refilled P116 samples at 3.5 Å resolution using cryoEM. The structure of the refilled P116 is practically identical at 3.5 Å resolution to the structure of the original P116 sample, including densities at the palm of the hand that can be assigned to ligands. Mass spectrometry of the refilled samples shows the clear presence of phosphatidylcholine and sphingomyelin lipids (**Figure 4**). Classes of subunits of the dimer show a wringing of ~80 degrees (**Supplementary Figure 5**, **Movie 3**).

P116 is conformationally flexible

In the original P116, empty P116 and refilled P116 samples, the structure appears predominantly as a homodimer. In all cases, the homodimer exhibits significant flexibility. Most prominently, the empty structure has a different arc radius than those of the original and

refilled structures. In the original and refilled structures, a wringing motion is visible: each monomer is twisted in the opposite direction along the axis perpendicular to the dimer axis (**Figure 2d**, **Movie 3**, **Supplementary Figure 5**). In all P116 structures, the N-terminal domain is the most flexible. Within the core domain, temperature factors are higher at the finger tips, indicating the movement of the antiparallel α-helices. When the fingers approach the palm, this results in a closing of the hand and a clash with the densities therein (**Movie 9**).

P116 ligands include essential lipids

We next set out to characterize the possible ligands within P116. We first measured the rate of radioactivity transfer to P116 after incubation with HDL particles containing either tritium-labeled cholesterol ([^{3}H]cholesterol) or tritium-labeled cholesteryl oleate as a representative of cholesterol esters (**Table I**). A significant fraction of the HDL-[^{3}H]-radiotracer was detected in the post-incubated and purified P116 fractions, indicating a net transfer of both cholesterol and cholesterol ester between HDL and P116. The total absence of the most abundant HDL protein (APOA1), cross-checked by immune detection, verified that no HDL remnants had contaminated the purified P116 fractions. The highest rate of radiotracer transfer was achieved when [^{3}H]cholesterol-containing HDLs were mixed with empty P116. Transfer of [^{3}H]cholesterol was also present, although reduced, when the original P116 was incubated with labeled HDL. Transfer of [^{3}H]cholesterol esters to P116 would require a direct interaction between HDL and P116, as these esters are buried in the core of the HDL particles (**Figure 4a** and **Table 1**). Passive cholesterol transport has been reported from cellular membranes to HDL or from LDL to HDL[16], but the concept that bacteria can exploit such a mechanism is completely new. The net flux of cholesterol is bidirectional and is governed by the cholesterol gradient between acceptor and donor molecules.

We then conducted a more detailed liquid chromatography-coupled mass spectrometry (LC-MS) analysis. We identified more than 500 lipid species in the samples and found striking differences between the original, empty and refilled P116 samples. In the empty P116 samples, a significantly reduced amount of lipids was detected (**Figure 4b and Supplementary Figure 6**). Characterization of the lipids in the original and refilled P116 samples showed the presence of phosphatidylcholine and sphingomyelin lipids, among others, which are essential for *M. pneumoniae*. While these analyses found wax esters in the original P116, far fewer were found in the refilled P116. Wax esters are not known to be required by *M. pneumoniae*, although some pathogenic bacteria use wax esters as a carbon source[17,18]. However, wax esters are part of the cultivation medium of the *E. coli* strain in which P116

was produced. These findings are in agreement with the fact that *M. pneumoniae* takes up and incorporates many lipid species and adapts its membrane composition to the available lipid spectrum. In the P116 samples refilled from FBS, a clear accumulation of the essential lipids phosphatidylcholine and sphingomyelin, as well as cholesterol molecules, can be seen (**Figure 4c, 4d** and **Extended Table 2**). These findings are in strong agreement with the functional data from the tritium-labeled cholesterol assay. Taken together, our lipidomics analyses revealed that P116 can bind to different lipid species. While purified P116 mainly carried PGs, PEs and wax esters, the refilled P116 preferentially bound to PCs, SMs, and cholesterols. Notably, the composition of the lipid species in the refilled P116 was strikingly different than the serum lipid distribution. For example, highly abundant uncharged TGs did not bind to P116. Thus, P116 although displaying a large bandwidth of lipid uptake, it does show a preference for selective lipid species (**Figure 4c, 4d** and **Extended Table 2**).

P116 binds HDLs between its N-terminal and core domains

Next, we performed cryoEM on a sample containing empty P116 and HDL. Of ~46,000 particles that were identified as HDL, ~25,000 were attached to P116. The resulting density at a resolution of 9 Å shows P116 interacting with HDLs at the region between the N-terminal domain and the core (**Figure 4f**). The density of P116 resembles the filled conformation, and the structure can be well fitted to the density map. Cryo-electron tomograms of whole *M. pneumoniae* cells indicate a similar arrangement of P116 with respect to the *Mycoplasma* membrane, although an unambiguous identification of the involved complexes is not possible due to the mediocre resolution (**Supplementary Figure 10**).

Summary

P116 is essential for the viability of the human pathogen *M. pneumoniae*[4] and is the target of a strong antigenic response in infected patients[19]. Its structure has a previously unseen fold with a uniquely large hydrophobic cavity filled with ligands. Mass spectrometry and radioactivity transfer experiments confirm a lipid exchange and identify these ligands as essential lipids. This structure, along with our insights into different P116 conformations and the P116 complex formation with HDL, reveals a mechanism by which *Mycoplasmas* extract lipids from their environment and most likely incorporate them by passive diffusion into their own membrane. In this mechanism, the structure of P116 changes according to the lipid cargo content in an apparently simple and newly discovered way for lipid transporters.

The transition from a full to an empty P116 molecule involves the closure of the hydrophobic cavity in concert with a wringing motion of the core domains. During this wringing motion, in which the monomers are each twisted in the opposite direction around their long axis, the hydrophobic cavities face almost opposite directions. The N-terminal domain is anchored in the *Mycoplasma* membrane, thus in vivo, the core domain is experiencing the high flexibility seen in our data sets. This enables a ratcheted motion in which one monomer of the core domain faces the *Mycoplasma* membrane and the other monomer faces the environment. This wringing motion can be repeated in a continuous manner. In this way, P116 could undergo a rolling movement on the *Mycoplasma* membrane, thus facilitating the passive transport of cholesterol and other essential lipids.

Mycoplasmas have a minimal genome and are capable of incorporating many different lipids into their membrane[7,8]. The lipid-binding versatility shown by P116 enables a single molecular system to cope with the transport of diverse lipids required by *Mycoplasmas*. Although only *Mycoplasmas* share genes with similar sequences to P116, other microorganisms that require uptake of lipids from the environment, including clinically relevant bacterial species such as Borrelia burgdorferi and Helicobacter pylori[9], may have similar systems to regulate their cholesterol homeostasis. Whether P116 shares functional similarities with other transfer proteins such as human cholesteryl ester transfer and phospholipid transfer proteins[20,21] requires further investigation. However, the diversity and amount of lipids that P116 can bind appear to be unmatched by any other known prokaryotic or eukaryotic lipid carrier.

Acknowledgements

We thank Laura Company and Irene Fernández-Vidal for their support during MALS and mass spectroscopy measurements, Antoni Iborra (Servei de Cultius Cel·lulars, Anticossos i Citometria, UAB) for his assistance with immunizing mice, and Rosa Pérez-Luque and David Aparicio for their constant support and discussions. We also thank the Central Electron Microscopy Facility, MPI of Biophysics in Frankfurt, which enabled us to collect the P116 empty dataset and in particular Sonja Welsch who assisted during the data collection. J.P. has been supported in part by grant BIO2017-84166-R from the Ministerio de Ciencia, Innovación y Universidades (Spain) to. I.F. was funded by Ministeriode Ciencia e Innovación (MICINN-Spain) grant PID2021-125632OB-C21. A.S.F. was supported by the Deutsche Forschungsgemeinschaft (FR 1653/14-1 for SM, FR 1653/6-3 for LS) and the Research Training Group iMOl (GRK 2566/1 for MPS).

Author contributions

DV: Project initiation; preparation of the P116 gene synthesis; cloning of two constructs 13-957 and 30-657; expression and purification tests; adapting the best conditions for its stabilization. Expression, purification of mutant W681A and analysis by MALS. DV, LS, IF, ASF: Model building of the original, emptied and refilled P116 protein. DV and JMC: Emptying protocol. On-site assistance in the experimental preparation of the HDL-P116 interaction and the uptake of radioactive cholesterol (free and esterified). LS: Planned and carried out the single particle analysis; solved the P116 structure in the original, emptied and refilled state; proposed the mechanism of cholesterol uptake based on the structural data; solved the structure of P116 with HDL; model building of the empty P116 protein. SM: Planned and carried out the single particle sample preparation for the empty, refilled and the sample mixed with HDL. J.P. and M.M Obtaining hybridomas and monoclonal antibodies vs P116 protein. Immunolocation of P116 by epifluorescence microscopy, time-lapse microcinematography. MS: Advised on single particle experiments and structure determination procedures. JDL and JMC: Mass spectrometry analysis of all samples prepared for single particle analysis; a complete lipidomics analysis. IF: Designed and supervised research. ASF: Designed and supervised research. IF and ASF: Prepared the manuscript, with contributions from all authors.

Author information

Cryo-electron microscopy densities of the original P116 density map (3.3 Å), the empty P116 (4 Å) and the refilled P116 (3.5 Å) have been deposited in the EM Data Base under the accession codes XXXX, XXXX and XXXX, respectively. Model coordinates of empty and original P116 have been deposited in the PDB under the accession codes YYYY and YYYY,

respectively. The authors declare no competing financial interests. Correspondence should be addressed to A.S.F. (achilleas.frangakis@biophysik.org) and I.F. (ifrcri@ibmb.csic.es).

References

1. Tsiodras, S., Kelesidis, I., Kelesidis, T., Stamboulis, E. & Giamarellou, H. Central nervous system manifestations of Mycoplasma pneumoniae infections. *The Journal of infection* **51,** 343–354; 10.1016/j.jinf.2005.07.005 (2005).
2. Jiang, Z., Li, S., Zhu, C., Zhou, R. & Leung, P. H. M. Mycoplasma pneumoniae Infections: Pathogenesis and Vaccine Development. *Pathogens (Basel, Switzerland)* **10**; 10.3390/pathogens10020119 (2021).
3. Razin, S., Yogev, D. & Naot, Y. Molecular biology and pathogenicity of mycoplasmas. *Microbiology and molecular biology reviews : MMBR* **62,** 1094–1156; 10.1128/MMBR.62.4.1094-1156.1998 (1998).
4. Lluch-Senar, M. *et al.* Defining a minimal cell: essentiality of small ORFs and ncRNAs in a genome-reduced bacterium. *Molecular systems biology* **11,** 780; 10.15252/msb.20145558 (2015).
5. Gaspari, E. *et al.* Model-driven design allows growth of Mycoplasma pneumoniae on serum-free media. *NPJ systems biology and applications* **6,** 33; 10.1038/s41540-020-00153-7 (2020).
6. Bittman, R. Mycoplasma membrane lipids. Chemical composition and transbilayer distribution. *Sub-cellular biochemistry* **20,** 29–52; 10.1007/978-1-4615-2924-8_2 (1993).
7. Leon, O. & Panos, C. Long-chain fatty acid perturbations in Mycoplasma pneumoniae. *Journal of bacteriology* **146,** 1124–1134; 10.1128/jb.146.3.1124-1134.1981 (1981).
8. Razin, S., Argaman, M. & Avigan, J. Chemical composition of mycoplasma cells and membranes. *Journal of general microbiology* **33,** 477–487; 10.1099/00221287-33-3-477 (1963).
9. Huang, Z. & London, E. Cholesterol lipids and cholesterol-containing lipid rafts in bacteria. *Chemistry and physics of lipids* **199,** 11–16; 10.1016/j.chemphyslip.2016.03.002 (2016).
10. Svenstrup, H. F., Nielsen, P. K., Drasbek, M., Birkelund, S. & Christiansen, G. Adhesion and inhibition assay of Mycoplasma genitalium and M. pneumoniae by immunofluorescence microscopy. *Journal of medical microbiology* **51,** 361–373; 10.1099/0022-1317-51-5-361 (2002).
11. Baseman, J. B., Cole, R. M., Krause, D. C. & Leith, D. K. Molecular basis for cytadsorption of Mycoplasma pneumoniae. *Journal of bacteriology* **151,** 1514–1522; 10.1128/jb.151.3.1514-1522.1982 (1982).
12. Krause, D. C., Leith, D. K., Wilson, R. M. & Baseman, J. B. Identification of Mycoplasma pneumoniae proteins associated with hemadsorption and virulence. *Infection and immunity* **35,** 809–817; 10.1128/iai.35.3.809-817.1982 (1982).
13. Gish, W. & States, D. J. Identification of protein coding regions by database similarity search. *Nature genetics* **3,** 266–272; 10.1038/ng0393-266 (1993).
14. Jumper, J. *et al.* Highly accurate protein structure prediction with AlphaFold. *Nature* **596,** 583–589; 10.1038/s41586-021-03819-2 (2021).
15. Washburn, L. R. & Somerson, N. L. Lipoproteins as substitutes for serum in Mycoplasma culture medium. *Journal of clinical microbiology* **10,** 586–589; 10.1128/jcm.10.4.586-589.1979 (1979).
16. Phillips, M. C. Molecular mechanisms of cellular cholesterol efflux. *The Journal of biological chemistry* **289,** 24020–24029; 10.1074/jbc.R114.583658 (2014).

17. Wältermann, M. & Steinbüchel, A. Wax ester and triacylglycerol inclusions. In *Inclusions in Prokaryotes*, edited by J. M. Shively (Springer-Verlag, Berlin/Heidelberg, 2006), Vol. 1, pp. 137–166.
18. Sirakova, T. D. *et al.* Wax ester synthesis is required for Mycobacterium tuberculosis to enter in vitro dormancy. *PloS one* **7,** e51641; 10.1371/journal.pone.0051641 (2012).
19. Drasbek, M., Nielsen, P. K., Persson, K., Birkelund, S. & Christiansen, G. Immune response to Mycoplasma pneumoniae P1 and P116 in patients with atypical pneumonia analyzed by ELISA. *BMC microbiology* **4,** 7; 10.1186/1471-2180-4-7 (2004).
20. Zhang, M. *et al.* Structural basis of the lipid transfer mechanism of phospholipid transfer protein (PLTP). *Biochimica et biophysica acta. Molecular and cell biology of lipids* **1863,** 1082–1094; 10.1016/j.bbalip.2018.06.001 (2018).
21. Zhang, L. *et al.* Structural basis of transfer between lipoproteins by cholesteryl ester transfer protein. *Nature chemical biology* **8,** 342–349; 10.1038/nchembio.796 (2012).
22. Köhler, G. & Milstein, C. Continuous cultures of fused cells secreting antibody of predefined specificity. 1975. *Journal of immunology (Baltimore, Md. : 1950)* **174,** 2453–2455 (2005).
23. Cedó, L. *et al.* LDL receptor regulates the reverse transport of macrophage-derived unesterified cholesterol via concerted action of the HDL-LDL axis: insight from mouse models. *Circulation research* **127,** 778–792; 10.1161/CIRCRESAHA.119.316424 (2020).
24. Mastronarde, D. N. Automated electron microscope tomography using robust prediction of specimen movements. *Journal of structural biology* **152,** 36–51; 10.1016/j.jsb.2005.07.007 (2005).
25. Punjani, A., Rubinstein, J. L., Fleet, D. J. & Brubaker, M. A. cryoSPARC: algorithms for rapid unsupervised cryo-EM structure determination. *Nature methods* **14,** 290–296; 10.1038/nmeth.4169 (2017).
26. Kunz, M. & Frangakis, A. S. Super-sampling SART with ordered subsets. *Journal of structural biology* **188,** 107–115; 10.1016/j.jsb.2014.09.010 (2014).
27. Kunz, M. & Frangakis, A. S. Three-dimensional CTF correction improves the resolution of electron tomograms. *Journal of structural biology* **197,** 114–122; 10.1016/j.jsb.2016.06.016 (2017).
28. Emsley, P. & Cowtan, K. Coot: model-building tools for molecular graphics. *Acta crystallographica. Section D, Biological crystallography* **60,** 2126–2132; 10.1107/S0907444904019158 (2004).
29. Afonine, P. V. *et al.* Towards automated crystallographic structure refinement with phenix.refine. *Acta crystallographica. Section D, Biological crystallography* **68,** 352–367; 10.1107/S0907444912001308 (2012).
30. Headd, J. J. *et al.* Use of knowledge-based restraints in phenix.refine to improve macromolecular refinement at low resolution. *Acta crystallographica. Section D, Biological crystallography* **68,** 381–390; 10.1107/S0907444911047834 (2012).
31. Guasch, A. *et al.* Structure of P46, an immunodominant surface protein from Mycoplasma hyopneumoniae: interaction with a monoclonal antibody. *Acta crystallographica. Section D, Structural biology* **76,** 418–427; 10.1107/S2059798320003903 (2020).
32. Vizarraga, D. *et al.* Immunodominant proteins P1 and P40/P90 from human pathogen Mycoplasma pneumoniae. *Nature communications* **11,** 5188; 10.1038/s41467-020-18777-y (2020).
33. Nakane, D., Kenri, T., Matsuo, L. & Miyata, M. Systematic structural analyses of attachment organelle in Mycoplasma pneumoniae. *PLoS pathogens* **11,** e1005299; 10.1371/journal.ppat.1005299 (2015).
34. Seto, S., Kenri, T., Tomiyama, T. & Miyata, M. Involvement of P1 adhesin in gliding motility of Mycoplasma pneumoniae as revealed by the inhibitory effects of antibody under

optimized gliding conditions. *Journal of bacteriology* **187,** 1875–1877; 10.1128/JB.187.5.1875-1877.2005 (2005).

Materials & Methods

Bacterial strains, tissue cultures and growth conditions

M. pneumoniae M129 strain was grown in cell culture flasks containing SP4 medium and incubated at 37°C and 5% CO_2. Surface-attached mycoplasmas were harvested using a cell scraper and resuspended in SP4 medium. To grow mycoplasma cells on IBIDI 8-well chamber slides, each well was seeded with about 10^5 CFUs and incubated for 12–24 h in 200 µL SP4 supplemented with 3% gelatin.

NSI myeloma cells[22] were grown in RPMI 1640 medium supplemented with 10% fetal bovine serum (FBS) and 50 µg mL^{-1} gentamycin (complete RPMI). Hybridomas were selected in complete RPMI supplemented with HAT media and BM-Condimed (Sigma Aldrich, St. Louis, USA).

Cloning, expression, and purification of P116 constructs

Regions corresponding to the MPN213 gene from *M. pneumoniae* were amplified from synthetic clones (**Supplementary Table III**) using different primers for each construct: $P116F_{30}$ and $P116R_{957}$ for P116(30–957); $P116F_{13}$ and $P116R_{957}$ for P116(13–957); $P116F_{212}$ and $P116R_{862}$ for P116(212–862); and $P116W_{681}$ to introduce mutation W681A (**Supplementary Table IV**). PCR fragments were cloned into the expression vector pOPINE (gift from Ray Owens; plasmid #26043, Addgene, Watertown, USA) to generate constructs, with a C-terminal His-tag. Recombinant proteins were obtained after expression at 22°C in B834 (DE3) cells (Merck , Darmstadt, Germany), upon induction with 0.6 mM IPTG at 0.8 OD600. Cells were harvested and lysed by French press in binding buffer (20 mM TRIS-HCl pH: 7.4, 40 mM imidazole and 150 mM NaCl) and centrifuged at 49,000 × *g* at 4°C. Supernatant was loaded onto a HisTrap 5 ml column (GE Healthcare , Chicago, USA) that was pre-equilibrated in binding buffer and elution buffer (20 mM TRIS-HCl pH: 7.4, 400 mM imidazole and 150 mM NaCl). Soluble aliquots were pooled and loaded onto a Superdex 200 GL 10/300 column (GE Healthcare, Chicago, USA)
in a protein buffer (20 mM TRIS-HCl pH 7.4 and 150 mM NaCl).

To obtain empty P116, 2.6% Triton X-100 was added to the protein sample and incubated for 1.5 h at room temperature. Subsequent purification followed the same methodology described above, but also included a wash step with the binding buffer plus 1.3% Triton X-100, followed by extensive washing with at least 20 column volumes of wash buffer (20 mM TRIS-HCl pH: 7.4, 20 mM imidazole) before eluting the samples from the

column. P116 was concentrated with Vivaspin 500 centrifugal concentrators (10,000 MWCO PES, Sartorius, Göttingen, Germany) to a final concentration of >0.5 mg/mL.

To refill P116 with lipids, the empty protein was incubated with approximately 1 ml FBS per mg P116 for 2 h at 30°C while still bound on the column. After extensive washing with at least 40 column volumes of wash buffer, elution and concentration were performed as described above.

HDL isolation and determination of cholesterol transfer rate

Human HDL (density 1.063–1.210 g/mL) was isolated from plasma of healthy donors via sequential gradient density ultracentrifugation, using potassium bromide for density adjustment, at 100,000 *g* for 24 h with an analytical fixed-angle rotor (50.3, Beckman Coulter, Fullerton, CA, USA). The amount of cholesterol and apolipoprotein A1 were determined enzymatically and by an immunoturbidimetric assay, respectively, using commercial kits adapted for a COBAS 6000 autoanalyzer (Roche Diagnostics, Rotkreuz, Switzerland). Radiolabeled HDLs were prepared as previously described[23]. Briefly, 10 μCi of either [1,2-^{3}H(N)] free cholesterol or [1,2-^{3}H(N)]cholesteryl oleate (Perkin Elmer, Boston, MA) were mixed with absolute ethanol, and the solvent was dried under a stream of N_2. HDL (0.5 mL, 2.25 g/L of ApoA1) was added to the tubes containing the radiotracers, as appropriate, and then incubated for 16 h in a 37°C bath. The labeled HDLs (both ^{3}H-cholesterol-containing and ^{3}H-cholesteryl oleate-containing HDLs) were re-isolated by gradient density ultracentrifugation at 1.063–1.210 g/mL and dialyzed against PBS via gel filtration chromatography. Specific activities of ^{3}H-cholesterol-containing and ^{3}H-cholesteryl oleate-containing HDLs were 1221 and 185 counts per minute (cpm)/nmol, respectively. The cholesterol transfer to P116 (1 g/L) was measured after adding either [^{3}H] free cholesterol-containing or [^{3}H]cholesteryl oleate-containing HDL (0.5 g/L of APOA1) and incubating for 2 h at 37°C. HDL and P116 were separated by a HisTrap HP affinity column. The radioactivity associated with each P116 and HDL fraction was measured via liquid scintillation counting. The percentage of [^{3}H]cholesterol transferred per mL was determined for each condition. The specific activities for each radiotracer were used to calculate the amount of free cholesterol and cholesteryl ester transferred from HDL to P116.

Size exclusion chromatography and multi-angle light scattering (SEC-MALS)

Molecular weights were measured from P116 samples using a Superose 6 10/300 GL (GE Healthcare, Chicago, USA) column in a Prominence liquid chromatography system (Shimadzu, Kyoto, Japan) connected to a DAWN HELEOS II multi-angle light scattering (MALS) detector and an Optilab T-REX refractive index (dRI) detector (Wyatt Technology, Santa Barbara, USA). ASTRA 7 software (Wyatt Technology) was used for data processing and analysis. An increment of the specific refractive index in relation to concentration changes (dn/dc) of 0.185 mL/g (typical of proteins) was assumed for calculations.

Matrix-assisted laser desorption/ionization-mass spectrometry (MALDI-TOF)

All samples were mixed in a 1:1 ratio with either DHB or sDHB (Bruker Daltonics, Germany) matrix solution (50 $mg \cdot ml^{-1}$ in 50% Acetonitrile (ACN), 50% water and 0.1% TFA). Subsequently 1 µl aliquots of the mixture were deposited on a BigAnchor MALDI target (Bruker Daltonics, Germany) and allowed to dry and crystallize at ambient conditions. Unless stated otherwise, all reagents and solvents were obtained from Sigma Aldrich, Germany.

MS spectra were acquired on a rapifleX MALDI-TOF/TOF (Bruker Daltonics, Germany) in the mass range from 20.000-120.000 m/z in linear positive mode and in the mass range from 100-1600 m/z in reflector positive mode. The Compass 2.0 (Bruker, Germany) software suite was used for spectra acquisition and processing.

Lipidomics analysis (LC-TIMS-MS/MS)

Samples were extracted using a modified MTBE/Methanol extraction protocol, and submitted to LC-nanoESI-IMS-MS/MS analysis using a Bruker NanoElute UHPLC coupled to a Bruker TimsTOF Pro 2 mass spectrometer operated in DDA-PASEF mode. In brief, 40 min gradients on PepSep C18 columns (1.9A, 75µm ID, 15cm length) were recorded in positive and negative ion mode. Data were analysed using the MS-DIAL pipeline (version 4.9).

Single-particle cryoEM

For single-particle cryoEM, a 3.5 µl drop of purified P116 (100–400 µg/mL in 20 mM Tris, pH 7.4 buffer or 600 µg/mL in 20 mM Tris, 2 mM CHAPSO, pH 7.4 buffer) or P116 mixed with HDL (250 µg/mL P116 and 1116 µg/mL HDL in 20 mM Tris, pH 7.4 buffer) was applied to a (45 s) glow-discharged R1.2/1.3 C-flat grid (Electron Microscopy Science, Hatfield, USA), and plunge-frozen in liquid ethane (Vitrobot Mark IV, Thermo Scientific,

Waltham, USA) at 100% relative humidity, 4 °C, nominal blot force –3, wait time 45 s, with a blotting time of 12 s. Before freezing, Whatman 595 filter papers were incubated for 1 h in the Vitrobot chamber at 100% relative humidity and 4°C.

Dose-fractionated movies of P116, P116 refilled and P116 mixed with HDL were collected with SerialEM v3.8[24] at a nominal magnification of 130,000x (1.05 Å per pixel) in nanoprobe EFTEM mode at 300 kV with a Titan Krios (Thermo Scientific, Waltham, USA) electron microscope equipped with a GIF Quantum S.E. post-column energy filter in zero loss peak mode and a K2 Summit detector (Gatan Inc., Pleasanton, USA). For P116, P116 refilled and P116 with HDL a total of 4376, 4019 and 3114 micrographs with 34, 29 and 30 frames per micrograph and a frame time of 0.2 s were collected. The camera was operated in dose-fractionation counting mode with a dose rate of ~8 electrons per $Å^2$ s^{-1}, resulting in a total dose of 50 electrons per $Å^2$ s^{-1}. Defocus values ranged from –1 to –3.5 µm.

For P116 empty, dose-fractionated movies were collected using EPU 2.12 (Thermo Scientific, Waltham, USA) at a nominal magnification of 105,000x (0.831 Å per pixel) in nanoprobe EFTEM mode at 300 kV with a Titan Krios G2 electron microscope (Thermo Scientific, Waltham, USA), equipped with a BioQuantum-K3 imaging filter (Gatan Inc., Pleasanton, USA), operated in zero loss peak mode with 20 eV energy slit width. In total 15,299 micrographs with 50 frames per micrograph and frame time of 0.052 s were collected. The K3 camera was operated in counting mode with a dose rate of ~ 16 electrons per A^2 s^{-1}, resulting in a total dose of 50 electrons per $Å^2$ s^{-1}. Defocus values ranged from -0.8 to -3.5 µm.

CryoSPARC v3.2[25] was used to process the cryoEM data, unless stated otherwise. Beam-induced motion correction and CTF estimation were performed using CryoSPARC's own implementation. Particles were initially clicked with the Blob picker using a particle diameter of 200–300 Å. Particles were then subjected to unsupervised 2D classification. For the final processing, the generated 2D averages were taken as templates for the automated particle picking, for the processing of P116 with HDL no template picking was performed. In total, 3,463,490, 4,532,601 particles, 2,930,863 particles and 262,981 particles were picked and extracted with a binned box size of 256 pixels for P116, P116 empty, P116 refilled and P116 with HDL respectively. False-positive picks were removed by two rounds of unsupervised 2D classification. The remaining 1,324,330 particles (P116), 1,140,275 particles (P116 empty), 1,311,526 particles (P116 refilled) and 46,277 particles (P116 with HDL) were used to generate an ab initio reconstruction with three classes followed by a subsequent heterogeneous refinement with three classes. For the final processing, 1,315,362 particles

(P116), 633,332 particles (P116 empty), 1,311,526 particles (P116 refilled) and 46,277 particles (P116 with HDL) were used. For the remaining particles, the beam-induced specimen movement was corrected locally.

The CTF was refined per group on the fly within the non-uniform refinement. The obtained global resolution of the homodimer was 3.3 Å (P116), 4 Å (P116 empty), and 3.5 Å (P116 refilled) (**Supplementary Figure 1 and Supplementary Table I**). To analyze the sample in regard to its flexibility the particles were subjected to the 3D variability analysis of cryoSPARC which was used to display the continuous movements of the protein.

Cryo-electron tomography of *M. pneumoniae*

M. pneumoniae M129 cells of an adherently growing culture were scraped in a final volume of 1 ml of SP4 medium and washed three times in PBS. This solution was mixed with fiducial markers (Protein A conjugated to 5 nm colloidal gold: Cell biology department, University Medical Center Utrecht, The Netherlands). From this stock a 3.5 µl drop was applied to a (45 s) glow-discharged R1.2/1.3 C-flat grid (Electron Microscopy Science, Hatfield, USA), and plunge-frozen in liquid ethane (Vitrobot Mark IV, Thermo Scientific, Waltham, USA) at 100% relative humidity, 4 °C, nominal blot force –1, with a blotting time of 10 s.

Tilt-series were recorded using SerialEM v3.8[24] at a nominal magnification of 105,000x (1.3 Å per pixel) in nanoprobe EFTEM mode at 300 kV with a Titan Krios (Thermo Scientific, Waltham, USA) electron microscope equipped with a GIF Quantum S.E. post-column energy filter in zero loss peak mode and a K2 Summit detector (Gatan Inc., Pleasanton, USA). The total dose per tomogram was 120 $e^-/Å^2$, the tilt series covered an angular range from -60° to 60° with an angular increment of 3° and a defocus set at -3 µm. Tomograms were reconstructed by super-sampling SART[26] with a 3D CTF correction[27].

P116 model building and refinement

The initial tracing of the core domain was performed manually with Coot[28]. It contained numerous gaps and ambiguities that were slowly polished by alternating cycles of refinement using the "Real Space" protocol in the program Phenix[29,30] and manual reinterpretation and rebuilding with Coot. The tracing and assignment of specific residues in the N-terminal domain were very difficult due to the low local resolution of the map for this domain, and only a partial interpretation was achieved. Using Robetta and AlphaFold [14] we obtained

different predictions of the N-terminal domain structure using different parts of the sequence. The highest ranked predictions, selected using the partial experimental structure already available, were obtained with AlphaFold for residues 81–245, which allowed us to complete the building of the N-terminal domain according to the cryoEM map. The RMS deviation between the AlphaFold prediction and the experimental model was 2.6 Å for 104 (63%) structurally equivalent residues. Some residues at the N-end of the N-terminal domain were difficult to identify and were represented as alanines in the final model. The whole P116 model was then refined using Phenix, and the final refined structure was deposited in the EMDB with code XXXX **(Supplementary Table II)**.

Polyclonal and monoclonal antibody generation

Two BALB/C mice were serially immunized with four intraperitoneal injections, each one containing 150 μg of recombinant P116 ectodomain (residues 30–957) in 200 μL of PBS with no adjuvants. The last injection was delivered four days before splenectomy. Isolated B lymphocytes from the immunized mice were fused to NSI myeloma cells[22] to obtain stable hybridoma cell lines producing monoclonal antibodies, as previously described[31] .Supernatants from hybridoma cell lines derived from single fused cells were first investigated by indirect ELISA screening against the recombinant P116 ectodomain. Positive clones were also tested by Western blot against protein profiles from *M. pneumoniae* cell lysates and by immunofluorescence using whole, non-permeabilized M. pneumoniae cells (see below). Only those clones with supernatants revealing a single 116 kDa band in protein profiles and also exhibiting a consistent fluorescent staining of *M. pneumoniae* cells were selected and used in this work. Polyclonal sera were obtained by cardiac puncture of properly euthanized mice just before splenectomy and titred using serial dilutions of the antigen. The titre of each polyclonal serum was determined as the IC_{50} value from four parameter logistic plots and found to be approximately 1/4000 for both sera. Polyclonal anti-P1 and anti-P90/P40 antibodies were obtained by immunizing two BALB/C mice with recombinant P1 and P90/P40 proteins[32], respectively, as described above. The titres obtained for polyclonal anti-P1 antibodies and anti-P90/P40 antibodies were approximately 1/2500 and 1/3000, respectively.

Immunofluorescence microscopy

The immunofluorescence staining of mycoplasma cells on chamber slides was similar to previously described[33], with several modifications. Cells were washed with PBS containing 0.02% Tween 20 (PBS-T) prewarmed at 37°C, and each well was fixed with 200 μL of 3%

paraformaldehyde (wt/vol) and 0.1% glutaraldehyde. Cells were washed three times with PBS-T, and slides were immediately treated with 3% BSA in PBS-T (blocking solution) for 30 min. The blocking solution was removed, and each well was incubated for 1 h with 100 µL of the primary antibodies diluted in blocking solution. For P116 polyclonal sera, we used a 1/2000 dilution; a 1/10 dilution was used for monoclonal antibodies from hybridoma supernatants. Wells were washed three times with PBS-T and incubated for 1 h with a 1/2000 dilution of a goat anti-mouse Alexa 555 secondary antibody (Invitrogen, Waltham, USA) in blocking solution. Wells were then washed three times with PBS-T and incubated for 20 min with 100 µL of a solution of Hoechst 33342 10 µg/µL in PBS-T. Wells were finally washed once with PBS-T and replenished with 100 µL of PBS before microscopic examination. Cells were observed by phase contrast and epifluorescence in an Eclipse TE 2000-E inverted microscope (Nikon, Tokyo, Japan). Phase contrast images, 4',6-diamidino-2-phenylindole (DAPI, excitation 387/11 nm, emission 447/60 nm) and Texas Red (excitation 560/20 nm, emission 593/40 nm) epifluorescence images were captured with an Orca Fusion camera (Hamamatsu, Hamamatsu, Japan) controlled by NIS-Elements BR software (Nikon, Tokyo, Japan).

Time-lapse microcinematography

The effect of anti-P116 antibodies and anti-P1 polyclonal serum on mycoplasma cell adhesion was investigated by time-lapse cinematography of *M. pneumoniae* cells growing on IBIDI 8-well chamber slides. Before observation, medium was replaced with PBS containing 10% FBS and 3% gelatin prewarmed at 37°C. A similar medium has been used to test the effect of P1 antibodies on mycoplasma adhesion and gliding motility[34]. After incubation for 10 min at 37°C and 5% CO_2, the slide was placed in a Nikon Eclipse TE 2000-E inverted microscope equipped with a Microscope Cage Incubation System (Okolab, Pozzuoli, Italy) at 37°C. Images were captured at 0.5 s intervals for a total observation time of 10 min. After the first 60 s of observation, the different antibodies were dispensed directly into the wells. The frequencies of motile cells and detached cells before the addition of antibodies were calculated from the images collected between 0 and 60 s of observation. The frequencies of motile cells and detached cells after the addition of antibodies were calculated from the images collected in the last minute of observation.

Table

Table I: Relative transfer of cholesterol and esterified cholesterol from HDL to P116

	% of [^{3}H]cholesterol transferred/mL	nmol cholesterol transferred/mL/h	nmol cholesterol transferred/mg P116 *
HDL to empty P116			
Free cholesterol	13.12	13.52	59.49 (6.3)
Esterified cholesterol	6.98	7.22	31.75 (3.3)
HDL to original P116			
Free cholesterol	7.89	7.42	32.63 (3.4)
Esterified cholesterol	6.32	6.01	26.44 (2.8)

* Numbers in parentheses are the estimated number of cholesterol molecules transferred per P116 subunit (assuming a Mw of ~105 KDa for the construct).

Figures

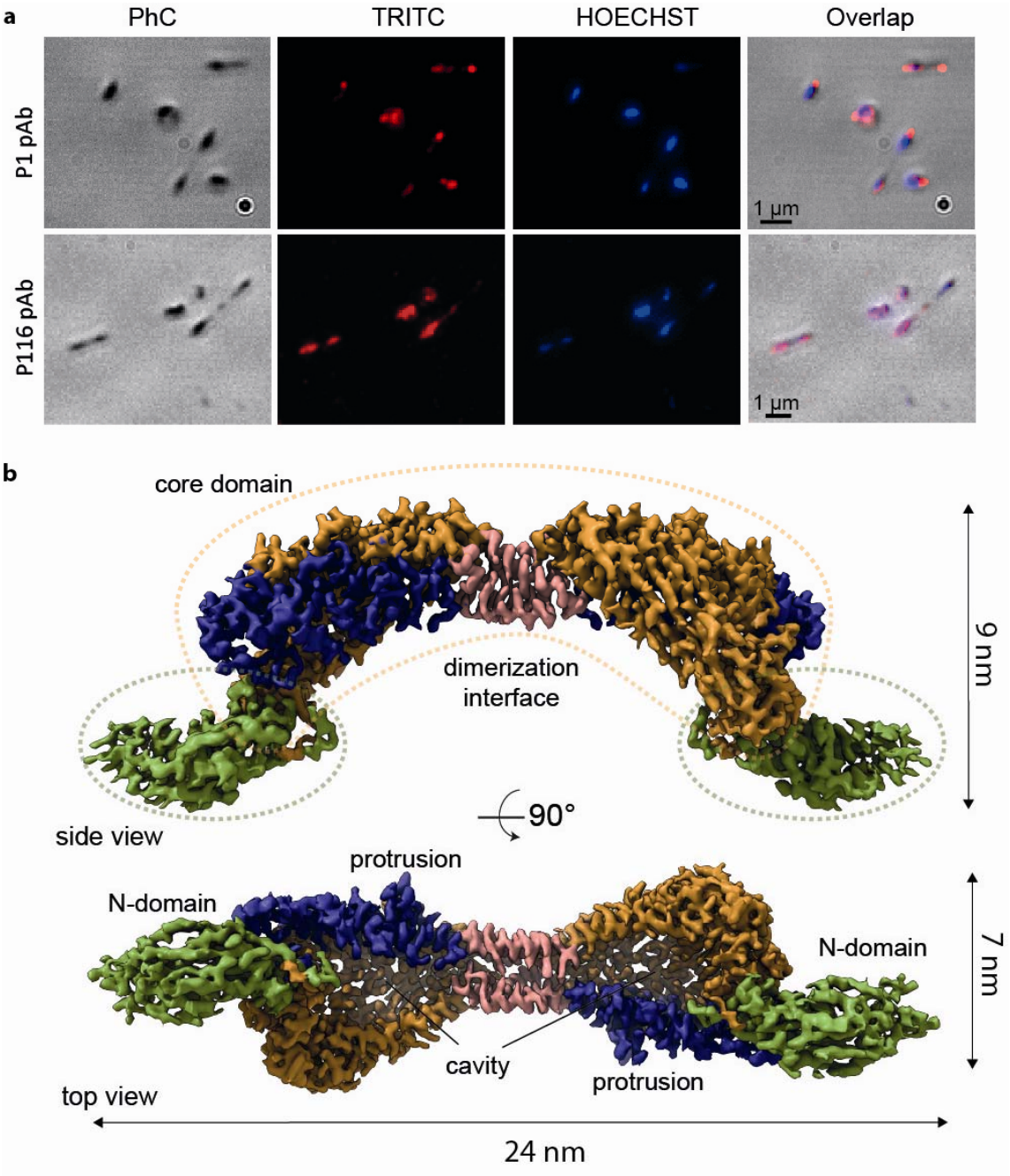

Figure 1. Structure of P116 and its localization in *Mycoplasma pneumoniae* cells. a) Phase contrast (PhC) immunofluorescence microscopy images *of M. pneumoniae* cells using labeling with polyclonal antibodies against the ectodomains of adhesin P1 (top row; used as a reference) and P116 (bottom row). Labelling for P1 concentrates at the tip of the cell, while for P116 it covers the whole surface homogenously. b) Two views of the cryoEM density map

of the complete extracellular region of the P116 dimer at 3.3 A□ resolution, 90 degrees apart. The homodimer is held together by the dimerization interface (shown in pink). The core domains have four contiguous antiparallel helices (shown in blue) and a β-sheet with five antiparallel strands (shown in orange). The N-terminal domain is shown in green. The top view displays a huge cavity that is fully accessible to solvent. The cleft providing access to the cavity spans the whole core domain. Each monomer also has a distinct protrusion (shown in blue as part of the antiparallel α-helices).

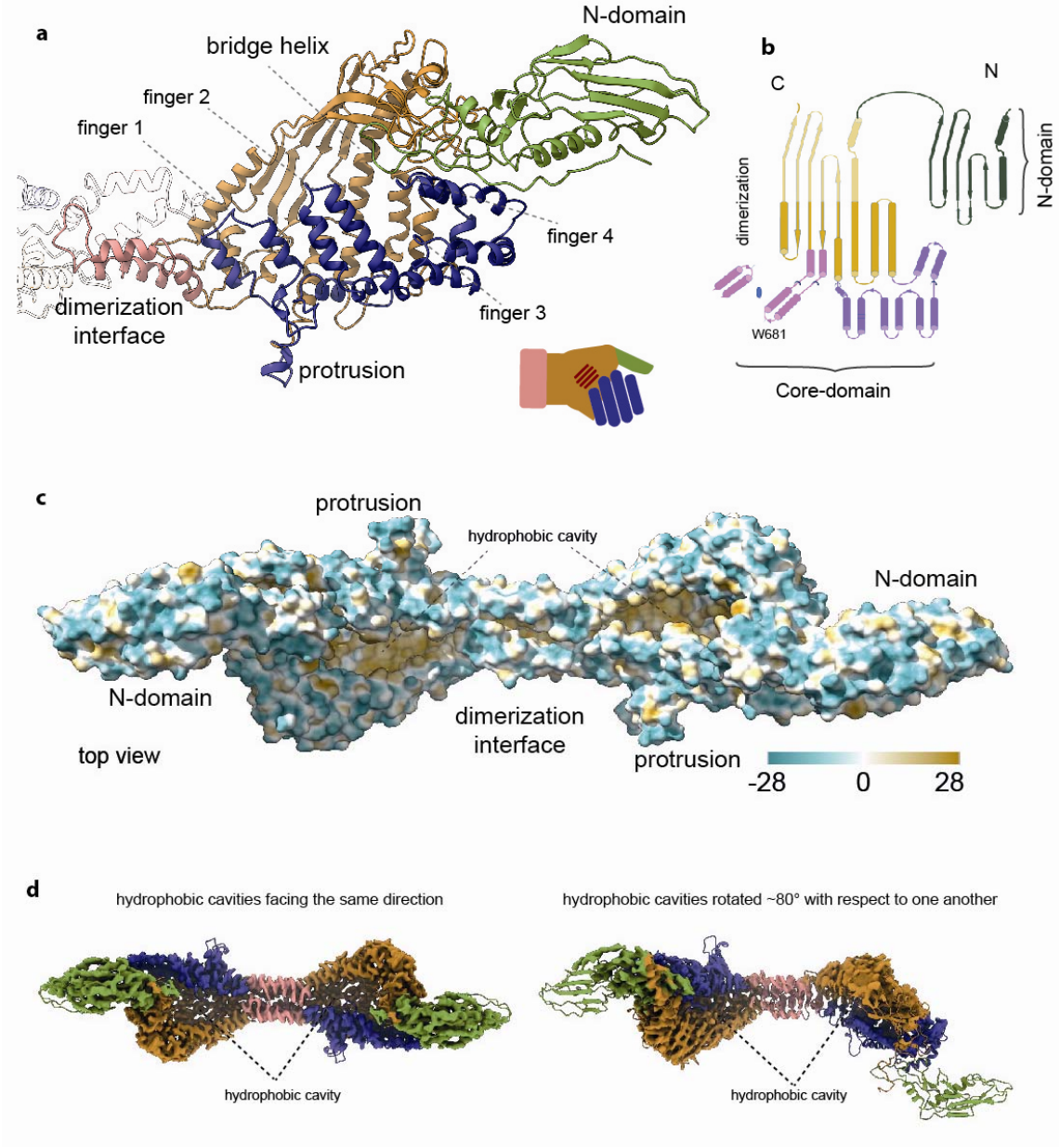

Figure 2. P116 structure and hydrophobic areas

a) Ribbon model of the P116 monomer, colored as in Fig. 1. The overall shape of the structure corresponds to a left hand, with the four antiparallel α-helices representing fingers (shown in blue), and the bridge helix and β-sheet of five antiparallel strands representing the palm. The N-terminal domain, which is very flexible, corresponds to the thumb. The dimerization helices (shown in pink) correspond to the wrist.

b) The overall topology of P116. The N-terminal and core domains of P116 share a similar topology, which suggests that P116 might have been generated by duplication of an ancestor domain**.**

c) The hydrophobic map of the P116 homodimer shows that the cavity in the core domain is hydrophobic and fully accessible to solvent.

d) CryoEM classes reveal a wringing movement of the P116 domain. Comparison of the two density maps shows that the wringing movement of P116 allows for the two hydrophobic cavities in the dimer to face almost opposite directions.

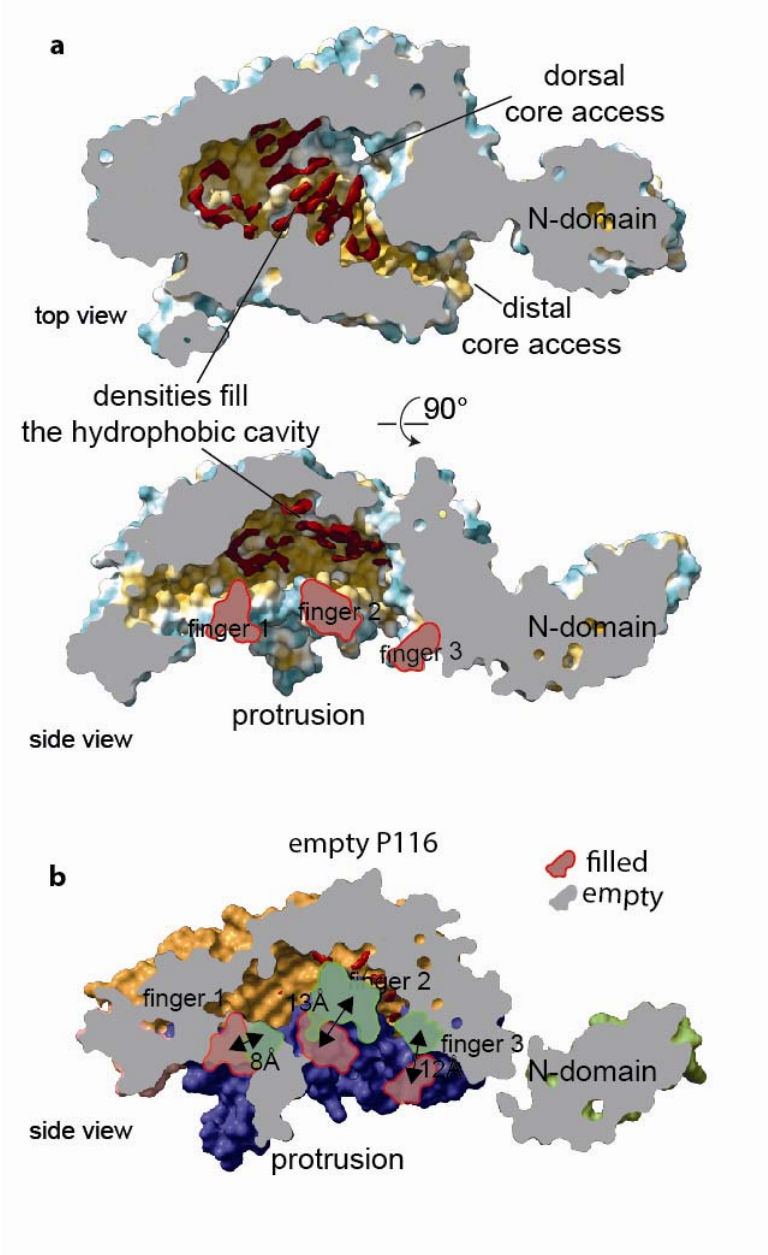

Figure 3: Purified P116 is filled with ligands and displays a large conformational variation compared to empty P116

a) Cross-section through the core domain of original P116 exposes a series of elongated densities (shown in red), which cannot be accounted for by the structure. These densities are ~4 Å wide and 10–19 Å long and are surrounded by highly conserved hydrophobic residues. The cross-section also reveals that the core domain can be accessed dorsally and distally. The side view of the core domain shows that the densities are aligned to the bridge helix and away from the fingers (shown in red).

b) The side view of the empty P116 shows a core domain that is significantly reduced in volume, with the positions of the fingers varying markedly from those in the structure of purified P116 (shown in green). For comparison, the position of the fingers in the original P116 are shown in red. Densities cannot be seen anymore and would generate steric clashes with the positions of the fingers.

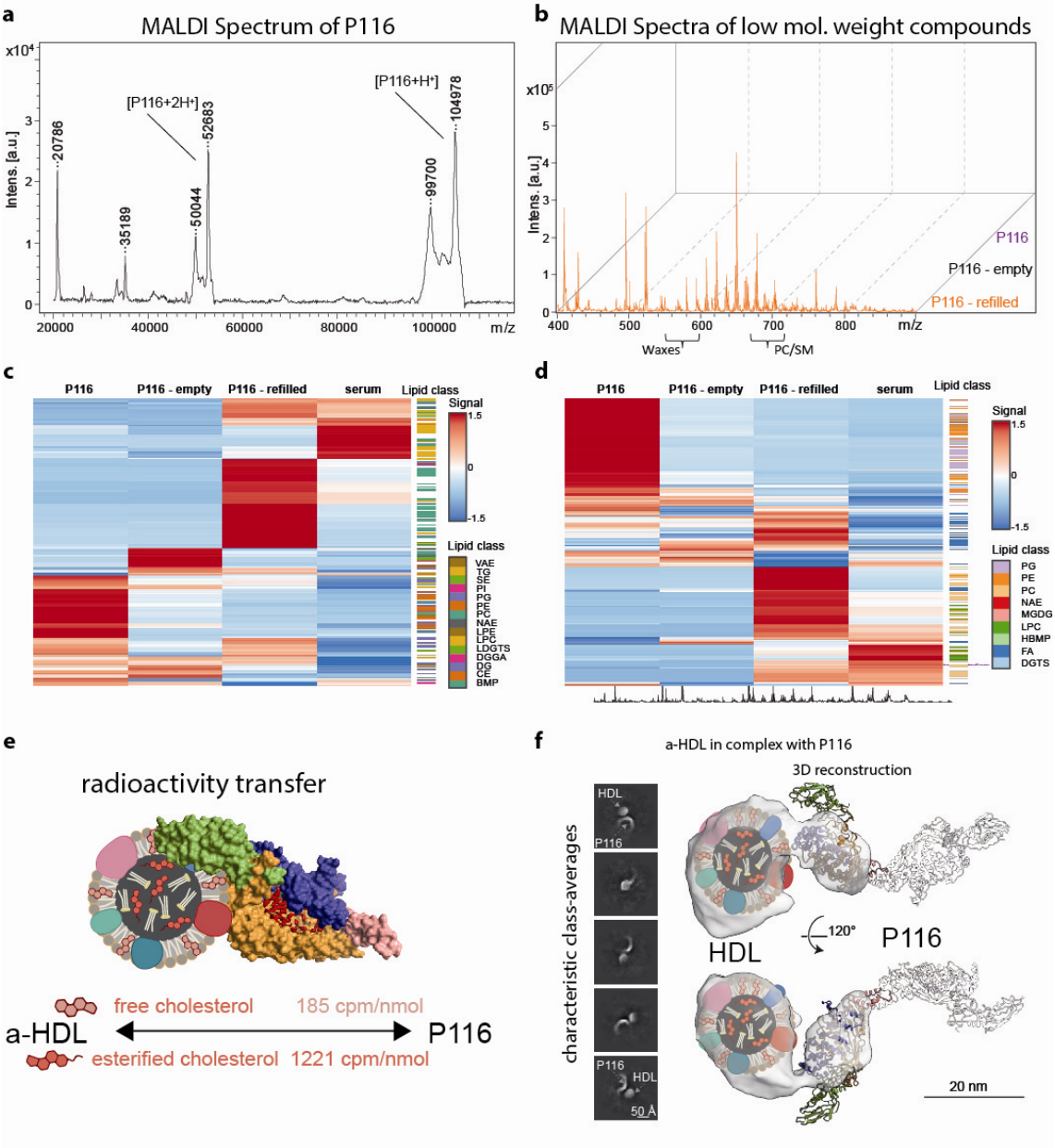

Figure 4:

a) MALDI-TOF mass spectrum of original P116 sample (linear mode, high mass range), showing a dominant peak at the 105 kDa corresponding to the singly charged full protein, as well as the charges states two, three and four. b) Stacked MALDI-TOF mass spectra (reflector mode, low mass range) of original P116 (purple, back), empty P116 (black, middle) and refilled P116 (orange, front) showing a change in the lipid distribution among the samples. c) and d) Hierarchical clustering of lipid compounds identified in positive (c) and negative (d) ion mode LC-ESI-IMS-MS/MS analyses, showing differential distributions of lipid compositions in original P116 (first column), emptied P116 (second column), refilled P116

(third column) and serum (fourth column), respectively. All data were normalized to the mTIC of all identified compounds in each sample and row-wise scaling was applied. e) When radiolabeled HDLs (here presented schematically) are incubated with P116, a net cholesterol transfer to P116 can be measured as indicated by the number at the flux arrow (for both free and esterified cholesterol). f) CryoEM analysis of empty P116 incubated with HDL shows that P116 binds HDLs between its N-terminal and core domains and is refilled. P116 is attached to HDL through its distal core access. Due to the flexibility of P116 and the variability of HDL, only one subunit of P116 can be seen at this threshold. Reducing the threshold causes the second subunit to appear.